

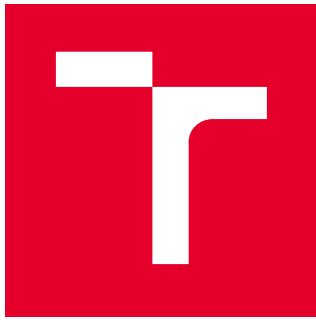
BRNO UNIVERSITY OF TECHNOLOGY

Faculty of Electrical Engineering
and Communication

MASTER'S THESIS

Brno, 2021

Bc. Diana Plišková



BRNO UNIVERSITY OF TECHNOLOGY

VYSOKÉ UČENÍ TECHNICKÉ V BRNĚ

FACULTY OF ELECTRICAL ENGINEERING AND COMMUNICATION

FAKULTA ELEKTROTECHNIKY
A KOMUNIKAČNÍCH TECHNOLOGIÍ

DEPARTMENT OF BIOMEDICAL ENGINEERING

ÚSTAV BIOMEDICÍNSKÉHO INŽENÝRSTVÍ

ANALYSIS OF NEURITE DIRECTIONALITY

ANALÝZA SMĚROVOSTI NEURITŮ

MASTER'S THESIS

DIPLOMOVÁ PRÁCE

AUTHOR

AUTOR PRÁCE

Bc. Diana Plišková

SUPERVISOR

VEDOUCÍ PRÁCE

Ing. Jan Odstrčilík, Ph.D.

BRNO 2021

Master's Thesis

Master's study program **Biomedical Engineering and Bioinformatics**

Department of Biomedical Engineering

Student: Bc. Diana Plišková

ID: 195732

**Year of
study:** 2

Academic year: 2020/21

TITLE OF THESIS:

Analysis of neurite directionality

INSTRUCTION:

1) Study the principle of scanning the neurons using a fluorescence microscope. 2) Carry out a literature review of works dealing with the analysis of fluorescence images of cells and nerve structures. 3) Design a suitable method for segmentation of neurites in available image data and implement it in the MATLAB programming environment. 4) Design and implement a method for analysis of neurite directionality. 5) Carry out an evaluation of the directionality analysis using a suitably designed methodology. 6) Discuss the achieved results and evaluate the effectiveness and usability of the applied solution. 7) Clearly comment on the created program functions.

RECOMMENDED LITERATURE:

[1] DIMA, A.; et al. Comparison of segmentation algorithms for fluorescence microscopy images of cells. Cytometry Part A, 2011, roč. 79, č. 7, s. 545-59.

[2] BAGLIETTO, S.; et al. Automatic Segmentation of Neurons from Fluorescent Microscopy Imaging. Biomedical Engineering Systems and Technologies, 2018, roč. 881, s. 121-133.

**Date of project
specification:** 8.2.2021

Deadline for submission: 21.5.2021

Supervisor: Ing. Jan Odstrčilík, Ph.D.

prof. Ing. Ivo Provazník, Ph.D.
Chair of study program board

WARNING:

The author of the Master's Thesis claims that by creating this thesis he/she did not infringe the rights of third persons and the personal and/or property rights of third persons were not subjected to derogatory treatment. The author is fully aware of the legal consequences of an infringement of provisions as per Section 11 and following of Act No 121/2000 Coll. on copyright and rights related to copyright and on amendments to some other laws (the Copyright Act) in the wording of subsequent directives including the possible criminal consequences as resulting from provisions of Part 2, Chapter VI, Article 4 of Criminal Code 40/2009 Coll.

ABSTRACT

The thesis is focused on the design of a suitable method for analyzing the directionality of neurites. Fluorescence microscopy images of neurons were used. Prior to segmentation, the images had to be preprocessed, using contrast adjustment, sharpening, and adaptive filtering using a Weiner filter. The individual proposals of segmentation methods consisted of simple thresholding, area growth and the use of morphological operations. Subsequent directionality analysis used the direction of the gradients in the image. The proposed method was also used as a classifier, which was able to segregate the respective images into classes according to the direction of the growth.

KEYWORDS

neuron, image processing, fluorescence microscopy, segmentation, analysis of directionality

ABSTRAKT

Práca je zameraná na navrhnutie vhodnej metódy analýzy smerovosti neuritov. Využité boli snímky neurónov z fluorescenčnej mikroskopie. Pred samotnou segmentáciou bolo potrebné snímky predspracovať, pričom sa postupne využila úprava kontrastu, ostrenie a adaptívna filtrácia pomocou Weinerovského filtru. Jednotlivé návrhy metód segmentácie pozostávali z prostého prahovania, narastaním oblastí a využitím morfológických operácií. Následná analýza smerovosti využívala smer gradientov v obraze. Navrhnutá metóda bola využitá aj ako klasifikátor, ktorý dokázal rozdeliť jednotlivé snímky do skupín podľa smeru rastu.

KĽÚČOVÉ SLOVÁ

neurón, spracovanie obrazov, fluorescenčná mikroskopia, segmentácia, analýza smerovosti

PLIŠKOVÁ, Diana. *Analysis of neurite directionality*. Brno, 2021, 47 p. Master's Thesis. Brno University of Technology, Faculty of Electrical Engineering and Communication, Department of Biomedical Engineering. Advised by Ing. Jan Odstrčilík, Ph.D.

ROZŠÍRENÝ ABSTRAKT

Úvod:

Nervová sústava je jedna z najdôležitejších častí ľudského tela. Riadi životné funkcie, závisí od nej pamäť, učenie a vedomie celého človeka. Základnou stavebnou jednotkou sú neuróny, ktorých špecifickou vlastnosťou je, že sa rodia procesom neurogenézy, primárne v embryu. Tým pádom je výskyt neurodegeneratívnej choroby u človeka neliečiteľný. Preto je veľmi dôležité skúmať neuróny v oblasti regeneratívnej medicíny. Ďalším prínosom analýzy neurónov je ich využitie v oblasti umelých neurónových sietí. Prvá kapitola práce popisuje anatomickú štruktúru neurónu, po ktorej nasleduje kapitola popisujúca základnú techniku vizualizácie neurónov, fluorescenčnú mikroskopiu. Obsahom kapitoly sú základné metódy ako wide-field a konfokálna mikroskopia. Takisto sú tam zhrnuté základné techniky farbenia pre lepšie pozorovanie neurónov. Ďalšou časťou práce sú kapitoly určené segmentácii a analýze smerovosti neurónov. Obsahujú základné metódy pre jednotlivé operácie ako napríklad aktívna kontúra a narastanie oblastí. V práci je takisto obsiahnutá kapitola popisujúca experimentálnu databázu, s ktorou sa pracovalo v praktickej časti. Metódy, ktoré boli použité v tejto práci sú popísané zvlášť v samostatnej kapitole. Výsledky praktickej časti sa nachádzajú v poslednej kapitole, ktorá obsahuje aj ich následnú diskusiu. Celú prácu ukončuje záver popisujúci zhrnutie celej práce.

Metódy:

Cielom práce bolo navrhnúť vhodnú metódu analýzy smerovosti v programovom prostredí Matlab. Predtým, ako bola aplikovaná metóda na snímky, bolo potrebné vytvoriť vhodnú metódu segmentácie. V tejto práci sú popísané až 3 metódy a ich porovnanie vhodnosti pre následnú analýzu smerovosti. Pred samotnou segmentáciou bolo potrebné spracovanie dát pre dosiahnutie čo najlepších výsledkov. Základom image preprocessingu bola úprava kontrastu, zaostrenie a odstránenie šumu z nasnímaných dát. Následne došlo už k aplikácii segmentačných metód. Prvá metóda pozostávala prevažne z prostého prahovania, druhá využívala princíp narastania oblastí za použitia inicializačného semienka. Posledná, tretia metóda, získavala binárny obraz za pomoci hranových detektorov a morfológických operácií. Čo sa týka presnosti a rýchlosti metódy, najlepšie obstála prvá metóda s využitím prostého prahovania. S takto získanými binárnymi obrazmi sa následne pracovalo pri vytváraní analýzy smerovosti. Metóda navrhnutá v tejto diplomovej práci spočíva v analýze gradientov obrazu. Každý obraz bol rozdelený na 117 podobrazov s veľkosťou 50x50 pixelov. Dôvodom tohto kroku bolo obmedzenie vplyvu dendritov vstupujúcich do sóm neurónov, kde dochádzalo k zlému výpočtu smeru gra-

dientu. Z jednotlivých podobrazov sa vypočítal smer gradientu, ktorého hodnota bola vložená do špecifickej premennej. Súčasťou analýzy bolo vytvorenie postupu, ktorý by zistil prevažujúci smer obrazu. Dôvodom toho boli vytvorené premenné, ktoré v sebe uchovávali jednotlivé hodnoty smeru gradientu. Po výpočte smerov v jednotlivých podobrazoch boli tieto hodnoty priradené do korešpondujúcich premenných. Najviac početná premenná bola označená ako premenná s prevládajúcim smerom, z čoho bola následne pomocou spriemerovania hodnôt vypočítaná jedna konkrétna hodnota smeru.

Výsledky:

Získané výsledky bolo potrebné porovnať s ground truth (GT) dátami, kvôli štatistickému vyhodnoteniu metódy. K dispozícii takéto dáta neboli, avšak pre túto prácu bol vytvorený pomocný program, cez ktorý užívateľ sám naklikal smery pre jednotlivé obrazy. Bolo vytvorených 5 sád GT, kde 5 jednotlivcov subjektívne naklikalo smer neurónov pre jednotlivé snímky. Keďže sa jednalo o nezávislých jedincov, každá naklikaná hodnota má rovnakú váhu voči všetkým datasetom a preto bola aj v rámci štatistiky vypočítaná stredná kvadratická chyba, aby bolo poukázané na rozdiely medzi jednotlivými sadami. Medzi jednotlivými GT dátami a výsledkami navrhutej metódy bola vypočítaná stredná kvadratická chyba (MSE). Dôvodom tohto výpočtu bolo získanie chybovosti medzi jednotlivými hodnotami GT spolu so získanými hodnotami. Výsledné hodnoty MSE môžu pôsobiť ako veľké, avšak pracuje sa s uhlami v intervale $\langle -180 - 180 \rangle$, pričom už aj 10° rozdiel medzi dátami môže nadobúdať vysoké hodnoty MSE, hoci smerovosť by bola vypočítaná správne. Pre určenie úspešnosti získaných uhlov bola vypočítaná priemerná hodnota všetkých GT sád v jednotlivých obrazoch a ich smerodajná odchýlka. Smerodajná odchýlka určovala hodnotu, s ktorou sa môže vypočítaný výsledok líšiť od priemernej hodnoty GT dát tak, aby bola ešte v medziach prijateľnosti, čo sa týka funkcionality navrhutej metódy. Po porovnaní vypočítaných dát s GT dátami a prihliadnutím na smerodajnú odchýlku, bola úspešnosť tejto metódy 83%. Navrhnutá metóda bola využitá aj ku klasifikácii neurónov podľa ich smeru rastu. Z dát, s ktorými sa pracovalo v tejto práci, bolo možné určiť 3 skupiny rastu smeru a to skupina, kde neprevládala žiadny smer, teda nebolo možné určiť, ktorým smerom neuróny na obrazoch rastú. Ďalšou skupinou boli neuróny, ktoré rástli smerom dolu a posledná skupina popisuje neuróny, ktoré rastú diagonálne/do štvorca. Klasifikačným kritériom pre jednotlivé snímky bol ich vypočítaný smer navrhnutou hodnotou. Táto klasifikácia mala presnosť 91%.

Záver:

Táto diplomová práca bola zameraná na analýzu smerovosti neuritov pomocou vhod-

nej metódy, ktorú bolo treba navrhnúť. Prvá kapitola popisuje stavbu neurónu, z ktorého sa skladá nervová sústava. Nachádzajú sa tam popísané jednotlivé časti a aká je ich funkcia. Druhá kapitola sa zaoberá fluorescenčnou mikroskopiou a jej využitie v pozorovaní neurónov. Nachádza sa tam princíp tejto techniky a aj jednotlivé typy, ako wide-field a konfokálna mikroskopia. Pre správne pozorovanie neurónov je potrebné využiť farbenie, keďže neurón nie je autofluorescenčný. Základné metódy farbenia sú taktiež popísané v tejto kapitole. V tretej kapitole sú popísané základné metódy segmentácie neurónov, konkrétne segmentácia somy a dendritov. V prípade segmentácie somy sa používa napríklad Laplacian of Gauss, v prípade dendritov growing region. Štvrtá kapitola sa zaoberá trasovaním neuritov, čo môže byť alternatívna verzia segmentácie. Obsahom piatej kapitoly je popis experimentálnych dát, ktoré boli využité k spracovaniu semestrálnej práce. Nachádza sa tam popis, ako boli neuróny vypestované a na akých štruktúrach. Šiesta kapitola popisuje praktickú časť diplomovej práce. Navrhnuté boli 3 rôzne metódy segmentácie a samotná analýza smerovosti neuritov. Posledná, siedma kapitola, popisuje získané výsledky a ich následnú diskusiu. Samotná metóda pri určovaní smerov rastu v porovnaní s ground truth dátami mala úspešnosť 83%. Keďže bolo viac sád GT dát, využívala sa smerodajná odchýlka, ktorá bola využitá ako orientačná hodnota, podľa ktorej sa určila hranica úspešnosti vypočítaných smerov metódy. Využitelnosť tejto metódy je aj v klasifikácii. Dáta boli rozdelené do 3 skupín, pričom presnosť klasifikácie bola 91%. V závere práce sú vložené príklady dát, kedy navrhnutá metóda bola schopná určiť správne smer a kedy nie, pričom je pri každom obraze popísané, kde mohla nastať chyba analýzy.

DECLARATION

I declare that I have written the Master's Thesis titled "Analysis of neurite directionality" independently, under the guidance of the advisor and using exclusively the technical references and other sources of information cited in the thesis and listed in the comprehensive bibliography at the end of the thesis.

As the author I furthermore declare that, with respect to the creation of this Master's Thesis, I have not infringed any copyright or violated anyone's personal and/or ownership rights. In this context, I am fully aware of the consequences of breaking Regulation § 11 of the Copyright Act No. 121/2000 Coll. of the Czech Republic, as amended, and of any breach of rights related to intellectual property or introduced within amendments to relevant Acts such as the Intellectual Property Act or the Criminal Code, Act No. 40/2009 Coll., Section 2, Head VI, Part 4.

Brno

.....

author's signature

ACKNOWLEDGEMENT

I would like to thank the supervisor of the master's thesis Ing. Jan Odstrčilík, Ph.D for his professional mentoring, consultations, patience, and thoughtful suggestions concerning the master's thesis.

Contents

Introduction	13
1 Neuron	14
1.1 Soma	14
1.2 Dendrites	14
1.3 Neurite	14
1.4 Telodendria	15
2 Fluorescence microscopy	16
2.1 Labeling of neurons	16
2.1.1 Green Fluorescent Proteins	16
2.1.2 Immunofluorescence	17
2.1.3 Brainbow	17
2.1.4 Tetbow	18
2.2 Wide-field microscopy	18
2.3 Confocal microscopy	18
3 Segmentation of neurons	20
3.1 Segmentation of cell	20
3.2 Segmentation of dendrites	22
4 Neurite tracing	23
5 Experimental database	24
6 Methods	25
6.1 Image preprocessing	25
6.2 Segmentation	26
6.3 Analysis of neurite directionality	27
6.4 Evaluation of the analysis	28
7 Results and discussion	30
Conclusion	39
Bibliography	40
List of symbols, quantities and abbreviations	43
List of appendices	44

A Tables containing ground truth data, standard deviation and calculated values.

List of Figures

2.1	Expression of fluorescent proteins in Peripheral Ganglia.	17
2.2	Mitral cells of the olfactory bulb labeled with Tetbow.	19
3.1	Neuron segmentation using 1st approach.	22
4.1	Neurite tracing	23
5.1	An example of data used in the thesis.	24
6.1	Comparison of input data and its output after image preprocessing. .	25
6.2	Comparison of outputs using individual methods.	27
6.3	Block diagram	28
7.1	MSE	31
7.2	Comparison of estimated directions by average GT values and com- puted values.	31
7.3	Example of original data belonging to respective classes.	32
7.4	Classification of data into individual classes according to the proposed method.	33
7.5	Classification accuracy	33
7.6	Output after direction analysis with correctly determined direction - downward.	34
7.7	Output after direction analysis with correctly determined direction - none.	35
7.8	Output after direction analysis with incorrectly determined direction.	36
7.9	Output after direction analysis with incorrectly determined direction.	37
7.10	Output after direction analysis with incorrectly determined direction.	38

List of Tables

7.1	Calculated MSE between individual ground truth datasets together with the proposed method.	30
A.1	Table of average value of ground truth data, standard deviation and calculated value for images 1 -36.	45
A.2	Table of average value of ground truth data, standard deviation and calculated value for images 37 -72.	46
A.3	Table of average value of ground truth data, standard deviation and calculated value for images 73 -100.	47

Introduction

The nervous system is one of the most important parts of the human body. It controls vital functions, memory, learning, and consciousness of the whole person depend on it. It is defined by a neuron, whose specific feature is that they are formed by the process of neurogenesis primarily in the embryo. Thus, the occurrence of neurodegenerative disease in humans is incurable. Therefore, it is crucial to study neurons in the field of regenerative medicine. Another use of neuronal analysis is its use in the field of artificial neural networks.

The first chapter describes the anatomical structure of the neuron, followed by a chapter describing the fundamental technique of neuron visualization, fluorescence microscopy. The chapter contains basic methods such as wide-field and confocal microscopy. It also summarizes the essential labeling techniques for better observation of neurons.

Another section of the thesis are chapters for segmentation and analysis of neural directionality. They contain basic methods for individual operations such as active contour, area growth and tracing.

The thesis also contains a chapter describing the experimental database, which was used in the practical part, i.e. what type of neurons were used and how they were grown. The methods that were used in this work are described separately in the chapter, which contains a detailed description of segmentation methods and the proposed method of directionality analysis. A total of 3 segmentation methods were suggested, from which only one was selected for the subsequent directionality analysis. The directionality results are described in the last chapter. This chapter is supplemented with regard to the use of the method in classification. The achieved results of the method are subsequently described and summarized in the discussion.

1 Neuron

A nerve cell or neuron is a basic functional unit of the nervous system whose task is to capture, process, and respond to a stimulus acting on the body. Nerve tissue is characterized by irritability, which means the formation, reception and sorting of the signal, and conductivity, which ensures their propagation. The number of neurons in the human body is in the tens of billions [1, 2].

It typically consists of the following parts:

- soma
- dendrites
- neurite
- telodendria

1.1 Soma

The body of a neuron, also called the soma or perikaryon, contains the nucleus. There are many cellular organelles in the cytoplasm, such as mitochondria, the Golgi apparatus, and lysosomes. Of particular importance is the rough endoplasmic reticulum, which is composed of cisternae. It is because of these clusters of cisternae that correspond in light microscopy to the basophilic beads, which are called Nissl bodies. By them, we can evaluate the functionality of the neuron [1].

1.2 Dendrites

Dendrites are short protrusions bulging from the body of a neuron. Their number ranges from one to tens or sometimes a hundred. It contains dendritic spines on which are synapses. The role of the dendrite is to receive nerve impulse. Afterward, it passes into the soma and thus into the nucleus of the neuron [1].

1.3 Neurite

The neurite, otherwise known as the axon, is one of the crucial parts of the neuron. Its function is to conduct nerve impulses. Therefore, it is the longest protrusion of a nerve cell to connect with other nerve cells or cells of other organs or tissues. There is only one neurite in the entire neuron, which can rarely be missing (amacrine cells in the retina). Its surface is covered by sheaths, which are divided into myelin sheath and neurilemma [1, 2].

Myelin sheath

Myelin sheath contains incisions (Ranvier nodes) that divide the sheath into internodes. Thanks to them, the conduction of nerve impulses is significantly accelerated. Because the sheath is electrically non-conductive, the only place that conducts impulses is the mentioned Ranvier nodes. This process of excitation is called saltatory conduction [1, 2].

Neurilemma

Neurilemma consists of Schwann cells that form a sheath on both myelinated and unmyelinated neurites. One cell is on neurites without a myelin sheath. Myelinated contain one cell at each internode [1, 2].

1.4 Telodendria

Telodendria are the final branches of the neurite. There are synapses through which a nerve impulse passes to another neuron or effector cell. We divide them into chemical and electrical.

Chemical synapses

Chemical synapses consist of a presynaptic end (telodendria), a synaptic cleft, and a postsynaptic membrane. The transmission of excitation takes place through mediators, which in the chemical synapse is performed by a neurotransmitter. It is located in the synaptic vesicles, which are located at the presynaptic end. The synaptic cleft refers to the intracellular space between two neurons or a neuron and a cell through which excitation is to pass. The postsynaptic membrane is a term describing the membrane of the neuron to which the excitation comes [1].

Electrical synapses

Electrical synapses are large-area connections through which an electric current passes directly. The difference between chemical and electrical synapses is the absence of synaptic vesicles. Another difference is the synaptic cleft, which is much smaller than the chemical one. As a result, the conduction of excitement is very fast [1].

2 Fluorescence microscopy

Fluorescence microscopy is a widely used type of microscopy in biology and the biomedical sciences. It is based on the detection and observation of fluorescent parts of substances. Specimen that have the property of fluorescence are called autofluorescent. This includes, for example, the amino acid tryptophan. However, not every specimen is autofluorescent and therefore are used fluorescent proteins such as green fluorescent protein. After application, we use its ability to emit visible light after irradiation with short-wavelength light in the ultraviolet (UV) region. This event is accompanied by the excitation of electrons to higher energy bands. After returning to the original band, a photon is emitted, which passes through a wavelength selective excitation filter. The wavelengths that pass through the excitation filter are reflected from the dichromatic mirror. They then travel through the microscope objective to the specimen, which they illuminate. If the specimen fluoresces, the emitted light passes back through the dichromatic mirror to the barrier (emission) filter, which is responsible for blocking unwanted wavelengths caused by excitation. In terms of construction, a fluorescence microscope differs from a conventional optical one by a modified condenser that is adapted to UV radiation [3, 4].

2.1 Labeling of neurons

Nerve cells, neurons, are not autofluorescent, so they do not emit radiation by themselves. Therefore, it is crucial to add substances that will emit radiation when illuminated at a specific wavelength. These substances must also bind to a particular place or places that we want to observe.

2.1.1 Green Fluorescent Proteins

One of the breakthroughs in biology and microscopy was the discovery of the green fluorescent protein (GFP). It was discovered by Osamu Shimomura in 1962 from the jellyfish *Aequorea victoria*, for which he and his colleagues were later awarded the Nobel Prize in Chemistry [5].

GFP is highly stable and produces significant fluorescence. The problem is its excitation maximum, 395 nm, which is close to the UV range (400 nm). UV light needs some optical attention because it can damage living cells. Therefore, it is not recommended to use GFP for imaging of living cells. This obstacle is removed in an enhanced form of GFP, enhanced GFP (EGFP), which has a shifted excitation maximum to 484 nm. This form is most commonly used for single-label fluorescent

protein experiments and is also one of the brightest currently available proteins. Other forms of GFP are, for example, Emerald, which has good photostability, and ZsGreen1. This protein comes from a coral reef with an emission maximum of 505 nm. It has been introduced as a replacement for EGFP but is very bright when applied to mammalian cells. Another disadvantage is that it has limited use in fusion images [6].

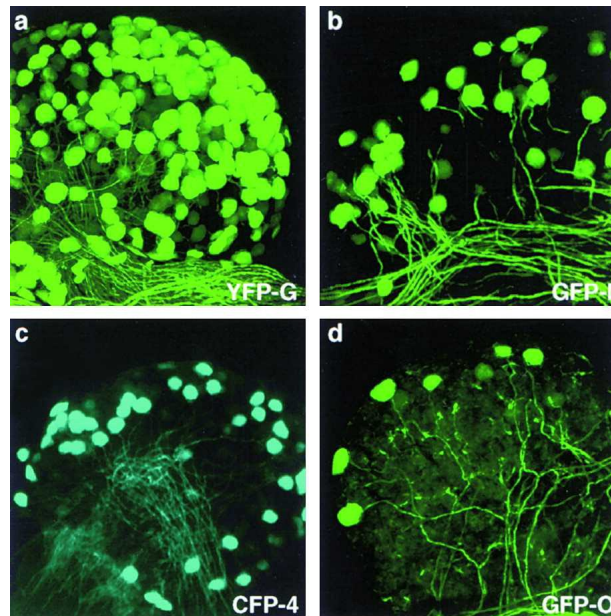


Fig. 2.1: Expression of fluorescent proteins in Peripheral Ganglia [7].

2.1.2 Immunofluorescence

Immunofluorescence (IF) is a method based on the principle of staining antibodies with immunoglobulins. This substance is mixed with synthetic fluorescent dyes and thus applied to cells or tissues. The advantage of the method is a good visualization of the protein and a high contrast of the observed specimen. The disadvantage is the need for fixation and permeabilization of the membrane before staining. Therefore, it is not suitable for observing living cells. IF is also an advantageous method for selecting a synthetic dye that fluorescents at different wavelengths. They can be combined with several direct labeling, and thus the resulting multicolor IF can visualize several cellular components at once [5].

2.1.3 Brainbow

Brainbow is a stochastic multicolor labeling method. It can label several neurons using three fluorescent proteins. It uses the Cre-IoxP system, which is specific re-

combination using deletion, insertion, translocation, and inversion. By introducing many copies of the transgene cassette, many color shades of the original three fluorescent proteins will be created using stochastic choices. The main disadvantage of this method is the limited use for neuronal tracing. The cause is the stochastic and combinatorial expression of fluorescent proteins, which is only possible with a low number of transgenes so that the expression level is not bright enough to observe high-resolution axons and dendrites [8].

2.1.4 Tetbow

Tetbow method is an improvement on the previous Brainbow method. It is a bright multicolor labeling method that produces more colors needed to track neurons over longer distances. It has enhanced expression, where it uses a tetracycline operating system, which ensures a higher level of expression. It uses plasmid or vector-mediated multicolor labeling. When Tetbow is combined with tissue clearing, 3D visualization of the structure of individual neurons is possible. Detergents, solvents, and heating are required to completely cleanse lipid-rich myelinated axons. However, these actions damage the tissue as well as the fluorescent proteins. Therefore, it is possible to use Tetbow with chemical tags, in which the encoded chemical tags have been labeled with a synthetic fluorophore and thus replaced fluorescent proteins. Tags such as SNAP or Halo form covalent bonds with the cognate substrate and the fluorescence remains stable even under rough clearing conditions [8].

2.2 Wide-field microscopy

This type of fluorescence microscopy shows the object over the entire area, so we can observe all the points simultaneously, which means faster imaging. Recently, light-emitting diodes (LEDs) have been used. Their advantage is long life and precise wavelength control. Because the resulting image is observed simultaneously, it is possible to record the image on the camera. The disadvantage is low contrast and spatial resolution, which is caused by focusing light on one image plane. Therefore, samples that are too thick or of various shapes are not suitable for observation because observation occurs outside the plane of focus. This imperfection can be compensated for by using thin layers of cells or macroscopic structures [9].

2.3 Confocal microscopy

The main advantage of confocal microscopy is the imaging of objects with greater thickness. Thus, the method is not limited to very thin samples as in the case of wide-

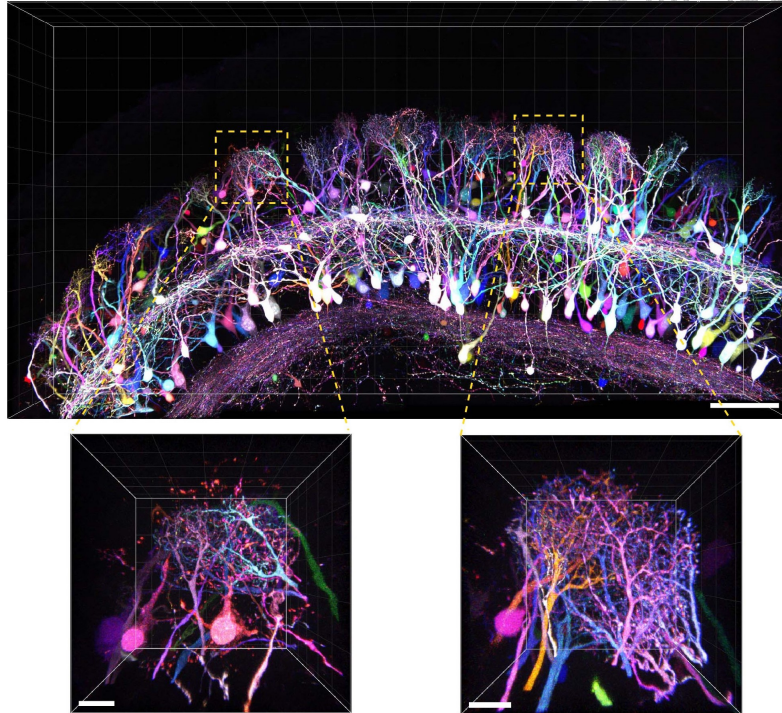


Fig. 2.2: Mitral cells of the olfactory bulb labeled with Tetbow [8].

field microscopy. The principles of excitation and emission apply to this method as well as to others. Compared to other methods of fluorescence microscopy, it differs in the excitation source, which is a laser, the method of sequential scanning of a point light source, and the method of detecting the intensity of emitted light, which has the function of a photomultiplier (PMT). The task of confocal microscopy is to get rid of unwanted out-of-focus light from the image. A pinhole aperture is intended for this purpose, which prevents the passage of unwanted light due to the transmission of only that light which corresponds to the confocal point in the sample where the excitation light was focused. This method constructs an image pixel by pixel by recording the fluorescence intensity at each point. This is possible thanks to the movement of oscillating mirrors, which optically focus the stationary laser and pinhole across the entire sample [9].

3 Segmentation of neurons

One of the main causes of neuronal monitoring is neurological diseases. Thanks to the great progress in microscopic technologies and their subsequent processing, we can observe their structure and morphological changes in the presence of diseases. Therefore, detection and segmentation of neurons are required. There are many approaches to begin segmentation of neurons or cells, but several procedures begin with the initialization of the nucleus or other region that will be the basis for further processing.

3.1 Segmentation of cell

One approach is to use a *Laplacian of Gaussian* (LoG) filter for initial detection. The method uses convolution with a Gaussian mask, resulting in a smoother image. It can be approximated by a mask, the size of which depends on the selected Gaussian variance σ^2 . After applying the threshold, we get a binary mask of the nuclei regions [10, 11].

Another method is *Multiscale Blob Enhancement Filtering*, which is used to identify areas where neurons are likely to be located. The method improves the intensity profile of the soma and reduces the influence of dendritic and neurite structures. It uses Hessian, which calculates the probability of which pixel belongs to a particular cell. Used blobness measurement corresponds to the equation (3.1) [12].

$$\mathcal{B}_s(x_0) = \begin{cases} 0, & \text{if } \lambda_1^{x_0,s} < 0 \\ e^{\frac{1}{2\beta^2} \left(\frac{\lambda_2^{x_0,s}}{\lambda_1^{x_0,s}}\right)^2}, & \text{otherwise} \end{cases} \quad (3.1)$$

where $\lambda_1^{x_0,s}$, $\lambda_2^{x_0,s}$ are eigenvalues of the Hessian matrix at the point x_0 at scale s . β is the threshold that determines the sensitivity of blob filter. Using multiscale filtration, we get the resulting blobness as a combination of the smallest and largest value of the scale, where the structures are still located [12].

After obtaining the region of interest (ROI), it is possible to apply *Active Contour*. Based on the energies, the active contour can determine the object from the background. It consists of external and internal energies that go against each other. External energy is a combination of forces due to the image that determines the position of the contour and internal energy to control changes. The shape of the resulting contour is defined by minimizing the energy functional. Since we have ROIs, energies are constructed locally at each point along the curve to analyze local regions. For each image, we can determine a radius equal to the average of the soma radius. A frequently used type of active contour is the snake model, which is

expressed by equation (3.2). The principle of the model is to change the shape and position of the curve while looking for a state of minimum energy. It searches local minimum in order to reduce the energy functional of the image [12, 13].

$$v_{(s,t)} = (x_{(s,t)}, y_{(s,t)}) \quad (3.2)$$

where x and y are the coordinates of the two-dimensional curve, v is spline parameter, which ranges in 0–1, s is linear parameter in range [0,1] and t is time parameter. After applying the method, we get a segmentation mask that tightly surrounds the cell body [13].

Another approach to neuronal segmentation include the use of an optimized *Mumford-Shah model*. Images must be normalized before processing. The segmentation itself begins using the Mumford-Shah model, which is region-based. Using the *Chan-Ves formulation* for two-phase segmentation, we can optimize the Mumford-Shah model. This optimization leads to an iterative procedure called the *Euler-Langer equation* [14]:

$$\phi^{t+\Delta t} = \phi^t + \Delta t \cdot \delta_\epsilon(\phi^t)[- \lambda_1(u_{(x,y)} - c_1)^2 + \lambda_1(u_{(x,y)} - c_2)^2] \quad (3.3)$$

where $u(x, y)$ is image intensity, λ_1 is the weight of contour features (length, area, foreground, and background), c_1 is the mean value of the background, c_2 is the mean value of foreground and δ_ϵ is a regularized Dirac delta function. The segmented nuclei will serve as references for cell segmentation. However, it is needed to initialize the level set function, which will look like [14]:

$$\phi_{(x,y)}^{n,t=0} = f_{(x,y)}^n - \left(\int f_{(x,y)}^n dx dy / \int dx dy \right) \quad (3.4)$$

where f^n represent the image intensities at pixel (x,y) corresponding to nuclei. Nuclei segmentation is obtained by substituting $u_{(x,y)}$ in the equation (3.3) for $f_{(x,y)}^n$ and evolving $\phi_{(x,y)}^{n,t}$. The evolution of the level set function for cell segmentation is modified as [14]:

$$\phi_{(x,y)}^{c,t=0} = f_{(x,y)}^c - 1 \quad (3.5)$$

where f^c represent the image intensities of fluorescent colors at pixel (x,y) corresponding to cell. Its segmentation is similar to nuclei, except that $u_{(x,y)}$ is substituted for $f_{(x,y)}^c$ in the equation (3.3 [14].

It may happen that due to fuzzy cell boundaries, they will cluster into one entity. A *Watershed Transformation* is applied to this problem, which divides the compressed cells into individual objects. This method describes segments as areas formed by certain neighborhoods that correspond to local minima in the image. These areas, also called catchment basins, correspond to the locus to which a drop, in our case a pixel, falls along the steepest descent path. We fill the basins with the

sorted pixels from lowest to highest, which are marked with the according basin. If there is a pixel marked by two basins, it is a border pixel. Finally, a size filter is applied that removes objects that do not fall within the soma size range [10, 12].

3.2 Segmentation of dendrites

In methods that segmented only the soma, it is also necessary to obtain peripheral parts, ie dendrites. A frequently used method is the *growing region method*. It is advantageous to have a segmented or detected section of neurons that serve as ROIs. This is followed by the segmentation of dendrites, where the method of region growing is used. The principle of growing region method is the choice of the initialization seed. It has typical properties, usually given by the parameter p , according to which other surrounding pixels are assigned if they meet a certain criterion of homogeneity. Each pixel belonging to the area analyzes its surroundings (4- or 8- connected) and compares the parameters of the pixels with the parameter of the seed, see the equation (3.6). If the condition is met, the pixel belongs to the segmented area [12].

$$|p_s - p_j| < T \quad (3.6)$$

where p_s is parameter of the seed, p_j is parameter of the particular pixel and T is threshold that was initially selected [12].

In the figure 3.1, we see a combination of methods: blob filtering, active contour, watershed transformation, and the growing seed.

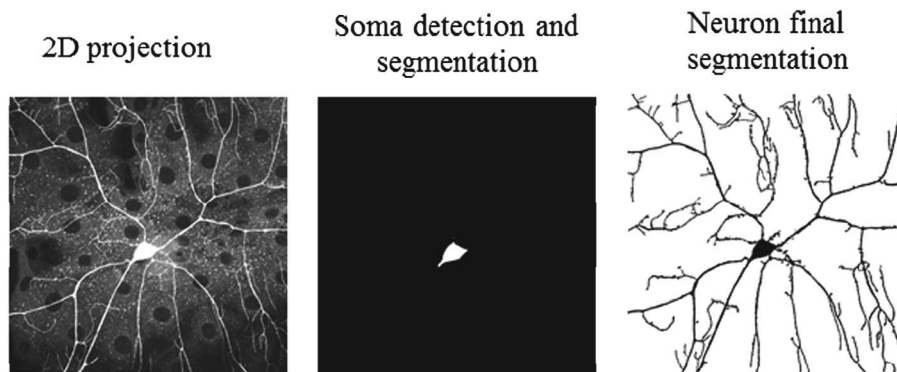


Fig. 3.1: Whole neuron segmentation [12].

4 Neurite tracing

Tracing the whole neuron, or parts of it are very important for research and quantitative analysis. The method consists of two phases: detection and linking. The classic depiction of neurons in the image is an elongated light part on a dark background. This fact is used by the detection phase, where we calculate for each pixel [15]

$$\mathbf{H}'_{f*G}(x) = \mathbf{H}_{f*G}(x) + \alpha \mathbf{R}_{\pi/2}^T \mathbf{H}_{f*G}(x) \mathbf{R}_{\pi/2} \quad (4.1)$$

where \mathbf{H}_{f*G} is the Hessian of the image to which the Gaussian blur filter has been applied and $\mathbf{R}_{\pi/2}$ denotes the rotation matrix with angle $\pi/2$. It is possible to use $\alpha = -1/3$, which determines the filter, which is maximally flat in the direction $\theta + \pi/2$. Subsequently, the eigenvalues are calculated, thanks to which we can obtain the neurite strength [15]

$$\rho = \begin{cases} \lambda(x)/\lambda_{min} & \text{if } \lambda(x) < 0 \\ 0 & \text{if } \lambda(x) \geq 0 \end{cases} \quad (4.2)$$

where λ is the larger value of the two eigenvalues and λ_{min} indicates the smallest lambda value of all the pixels in the image. To connect consecutive pixels, it is necessary to calculate the cost of moving from pixel x to any other 8- connected pixel y [15]

$$C(x, y) = \gamma C_\lambda(y) + (1 - \gamma) C_v(x, y) \quad (4.3)$$

where $\gamma \in [0, 1]$ is a parameter determining the relative weight of C_λ and C_v . The normalized cost components C_λ and C_v are defined as follows [15]

$$C_\lambda(y) = 1 - \rho(y) \\ C_v(x, y) = \frac{1}{2} \{ \sqrt{1 - \varphi(x, y)} + \sqrt{1 - \varphi(y, x)} \} \quad (4.4)$$

where $\varphi(x, y) = |v(x) \cdot d(x, y)|$, with $v(x)$ as normalized eigenvector and $d(x, y)$ as the unit vector in direction $y - x$. The resulting paths are obtained by Dijkstra's shortest-path algorithm. The figure 4.1 shows the output of neurite tracing [15].



Fig. 4.1: Output of the neurite tracing algorithm [15].

5 Experimental database

The data we work within the thesis are hippocampal neurons that have been isolated from rat brains. Because neurons require coating, the structures (test substrates) were coated with poly-D-lysine for one hour. Subsequently, after rinsing the structures with deionized water, neuron seeding took place. Two structures were used, namely quartz grooves and parylene cues on quartz substrate. The reason for the use of these structures is inspired by biological conditions within the development of the nervous system. One of the factors that migrate neurons is scaffold tracts formed from glia cells. For *in vitro*, said structures were used as a variation of glia scaffolds [16].

Neurons were stained 7 days after cultivation using Anti-NeuN and Anti-Rabbit IgG antibodies. The data were acquired using fluorescent mode, where the neural morphology is clearly visible. The data set used in the thesis contains diverse 100 images displaying neural growth in various directions as can be seen in the Fig.5.1 [16].

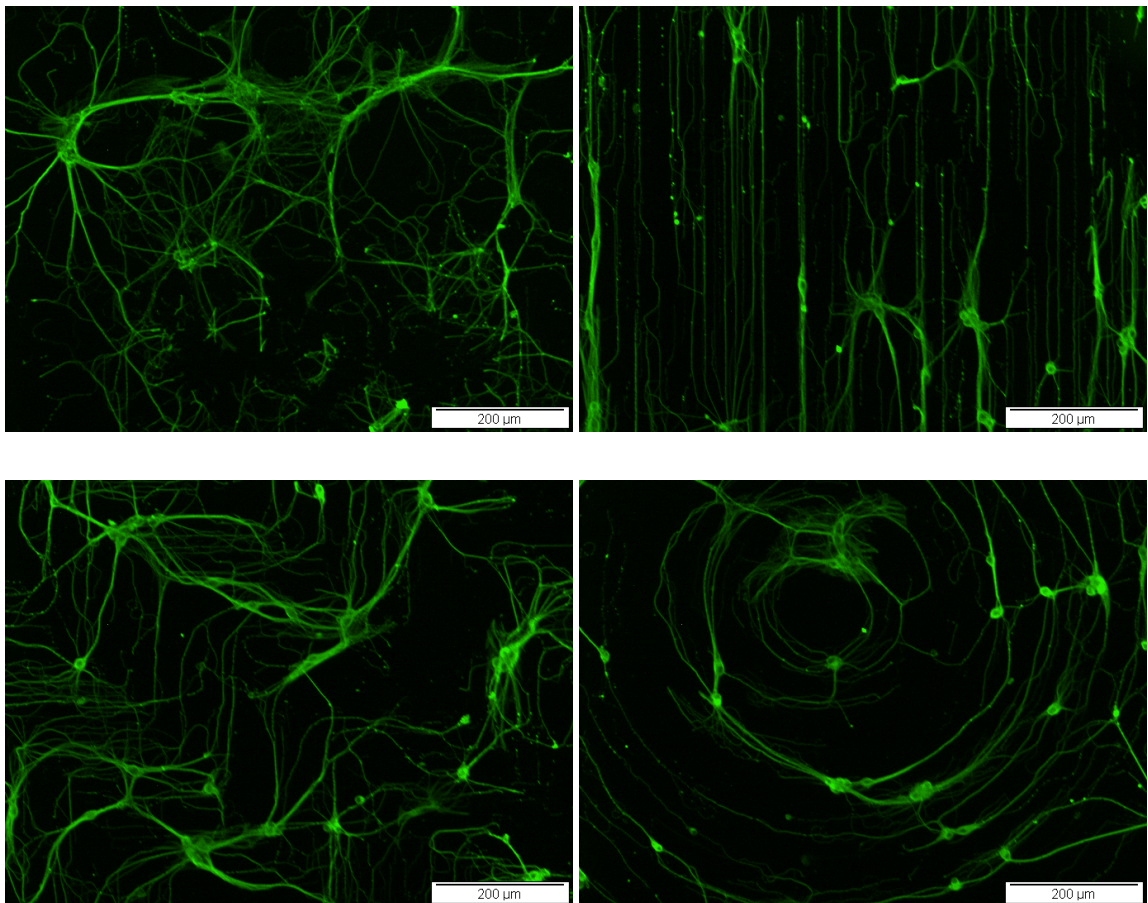


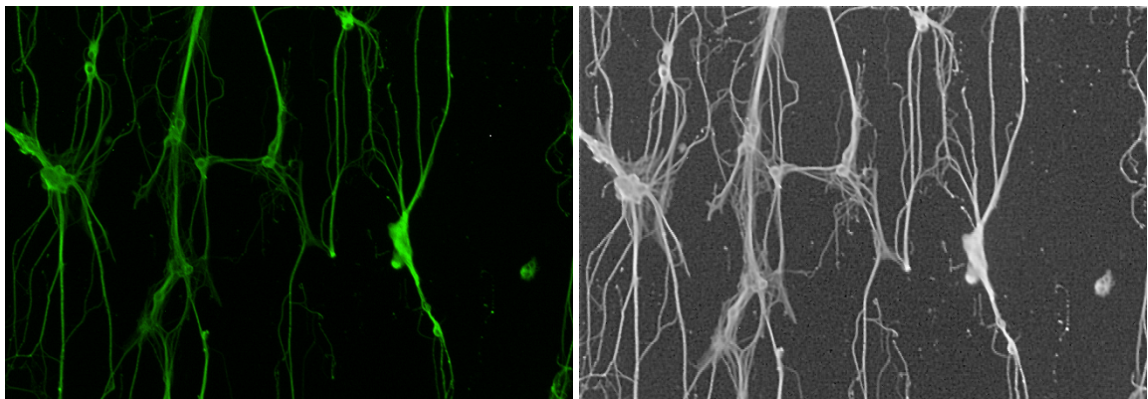
Fig. 5.1: An example of data used in the thesis.

6 Methods

The objective of the work was to design a suitable method of directionality analysis in the Matlab programming environment. Before the method was applied to the images, a suitable segmentation method had to be developed. This work describes up to 3 methods and their comparison of suitability for subsequent analysis of directionality. Prior to the segmentation itself, data preprocessing was necessary to achieve the best possible results.

6.1 Image preprocessing

The basis of image preprocessing was the adjustment of contrast, focusing, and removal of noise from the scanned data. The read image was converted to grayscale to which a gamma correction with a gamma value of 0.5 was applied. It is a non-linear operation, thanks to which we increased the brightness, which made it possible to make parts of the neurites visible. Subsequently, the sharpening method was applied. The principle is to use a 2D image convolution with an averaging mask, which gives a blurred image. By subtracting from the original image, we get details, which correspond to parts of the image different from the background. We add these details to the original image. By using the contrast enhancement, we adjusted the intensity values by saturating the pixels. These operations also caused noise enhancement, which we filter using a 2D Wiener filter. This is an adaptive filtration using a low-pass filter. The resulting image after preprocessing is shown in the Fig.6.1.



(a) Example of input data.

(b) Input data after image preprocessing.

Fig. 6.1: Comparison of input data and its output after image preprocessing.

6.2 Segmentation

The first approach was the thresholding method. It is a very simple and intuitive method, where using the input data we can create a binary image, according to a specified threshold. In this method, the threshold was determined using Otsu's method [17]. The principle of this method is to convert the image to binary according to the selected threshold, which in Otsu's method is intended as minimizing or maximizing the variance between inter-classes. According to this threshold, it determines which pixels belong to the background and which describe the object. We applied a morphological erosion operation to the binary image, which eliminated isolated points in the background. Subsequent application of a 2D median filter reduced background noise.

The second approach was to use a growing region method using an initialization seed. This algorithm was described in section 3.2 Segmentation of dendrites. In this work, a static criterion was used, which compared the intensity values of the current pixel with the initial one. The criterion value was determined as the difference between the maximum pixel intensity and the pixel intensity value that fell within the neurite area of interest. If the difference in intensity values is greater than the specified threshold, it is a dark pixel, which in this case resembles the background.

The third approach used edge detection. To prevent the detection of background noise, we used semi-thresholding, where the values of pixel intensities smaller than the threshold were defined as 0, i.e. they represent the background. The threshold was determined from the histogram of the image, where we chose the value of the area of interest. Edge detection was used on the semi-thresholded image with a Canny detector. It finds the edges by searching for local maximum of the image gradient. There are two thresholds for detecting weak and strong edges. Afterward, morphological operations were applied, namely, closing and dilatation. These methods filled parts of the area of interest of neurites. Eventually, a 2D median filter was applied using 10x10 mask, which was determined experimentally.

The output data for which the individual methods were applied can be found in Fig.6.2. By comparison, we see that the best segmentation is obtained using the thresholding method. Although not all parts of the neurites are perfectly segmented, this procedure is the most accurate by comparison with the remaining methods. The growing region method is also of good quality, but its limitation lies in the manual selection of the initialization seed, with only one being selectable. Removing these restrictions could improve the quality of segmentation. The last approach used edge detection, wherein Fig.6.2 is shown, there has been an artificial increase in the area of neurites. This is caused by the filling of areas that do not belong to each other.

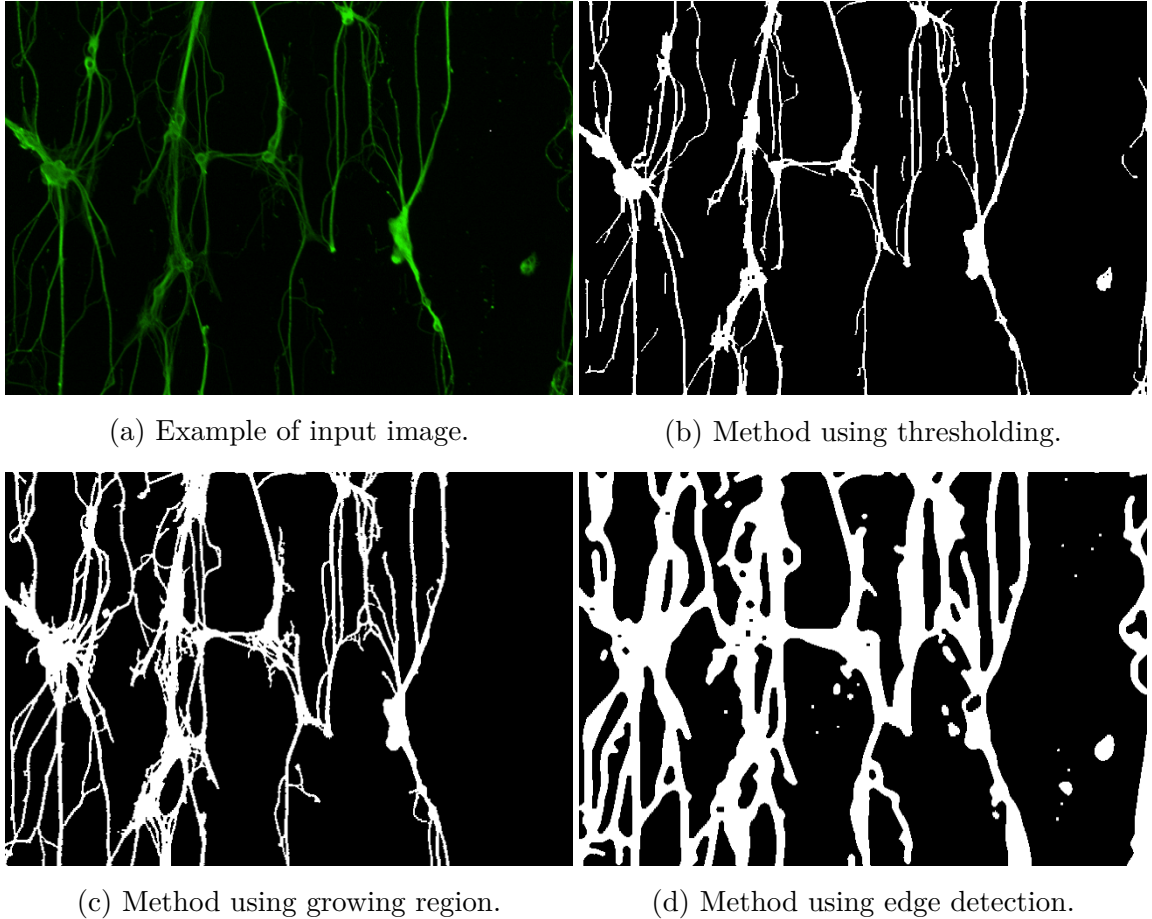


Fig. 6.2: Comparison of outputs using individual methods.

6.3 Analysis of neurite directionality

The essence of the master's thesis was the design and implementation of a suitable method for neurite directionality analysis. The proposed method consists in the analysis of image gradients. The gradient describes the steepness, the slope of the function, which was used in the work. Since the gradient is very sensitive to each pixel in the image, the simple thresholding segmentation method was used. Each image was divided into 117 sub-images with a size of 50x50 pixels. The reason for this step was to limit the effect of dendrites entering the soma of neurons, where the gradient direction was calculated incorrectly. The direction of the gradient was estimated from the individual sub-images, the value of which was inserted into a specific variable. Part of the analysis was to create a procedure that would determine the predominant direction of the image. Therefore, variables were created that held the individual values of the gradient direction. They carry only a certain direction that belongs to them. They were generated from 180° to -180° , where 0° corresponded to the x-axis. The variables with positive values were generated by 20°

and the variables consisting negative values were generated by 2° . The reason for this decision was the assumption of downward growth. After calculating the directions in the individual sub-figures, these values were assigned to the corresponding variables. The most numerous variable was marked as a variable with a predominant direction, from which one specific value of the direction was subsequently calculated by means of averaging the values. The whole procedure of the proposed method is shown by the individual steps in the block diagram in the Fig.6.3.

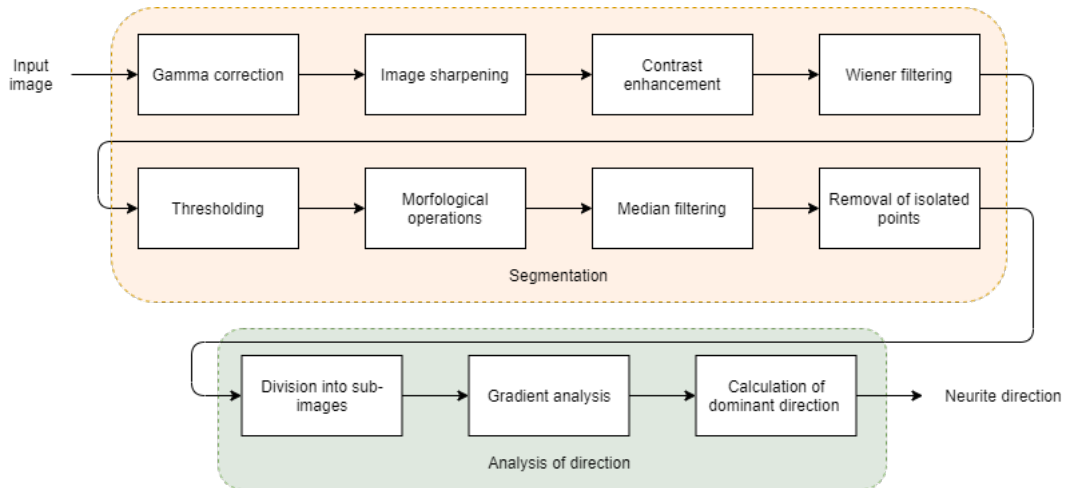


Fig. 6.3: Block diagram of proposed method.

6.4 Evaluation of the analysis

In order to evaluate the success rate of the method and its results, statistical estimators were used, namely the mean squared error and the standard deviation. The reason for choosing these methods was the occurrence of several ground truth datasets and therefore it was necessary to compare the values both between the individual ground truth datasets and between the computed values of the proposed method. A more detailed description of the explanation can be found in the chapter 7 Results and discussion.

Standard deviation

The standard deviation (SD) indicates the variation or variance of the data set, i.e. how far the values are from their mean. It always acquires a positive value or zero. If the SD is small, the values in the dataset are close to the mean value, if the SD is high, the values are more distributed from the average, so the data in the set show

more variation. Formula for SD [18]:

$$\sigma = \sqrt{\frac{\sum(x - \bar{x})^2}{n - 1}}, \quad (6.1)$$

where x is number, \bar{x} is mean, average value and n is number of data [18].

Mean squared error

The mean squared error (MSE) determines the error rate of the function as the difference between the estimated values and the actual ones by calculating their mean square difference. Always gains positive values. The larger the MSE, the more the values will differ and vice versa. Formula for calculating MSE [19]:

$$MSE = \frac{1}{n} \sum(x - \hat{x})^2, \quad (6.2)$$

where x means observed value, \hat{x} predicted value and n number of data [19].

7 Results and discussion

The obtained results had to be compared with ground truth data in order to be able to statistically evaluate this method as accurate or inaccurate. This type of data were not available, however a supplementary program was created for this work, through which the user clicked the directions for individual images. 5 sets of ground truth (GT) data were created, where 5 individuals subjectively estimated the direction of the neurons for each image. Since there were 5 independent individuals, each approximated value had the same weight for all datasets, and therefore the mean square error was calculated to point out the differences between the individual sets. As shown in the Tab.7.1, the MSE was also calculated between each dataset and proposed method. For better interpretation, a graphical display was also created, Fig.7.1, where we see that GT_2 has the highest error rate within all data. The remaining GT data together with the proposed method have approximately similar values. At first glance, the MSE values seem too large, but the whole method works with angles in the range $-180^\circ - 180^\circ$. Thus, even the 10° difference between two GT sets acquires large MSE values, although both sets estimate a very similar direction. GT_1 has the most similar values with the values of the proposed method, while MSE is 176.81. The reason for the high MSE is the fact that individuals indicated directions in images where there were many neural structures and not every image had a visible direction of growth.

Tab. 7.1: Calculated MSE between individual ground truth datasets together with the proposed method.

MSE	GT_1	GT_2	GT_3	GT_4	GT_5	Method
GT_1	0,00	489,32	142,81	70,89	149,20	176,81
GT_2	489,32	0,00	299,31	391,62	311,84	593,24
GT_3	142,81	299,31	0,00	101,76	107,46	269,91
GT_4	70,89	391,62	101,76	0,00	126,88	229,82
GT_5	149,20	311,84	107,46	126,88	0,00	197,39
Method	176,81	593,24	269,91	229,82	197,39	0,00

In order to determine with which value to compare the obtained values calculated by the method, the average value of all GT sets in the individual images and the standard deviation were estimated. The standard deviation determined the value with which the computed result could differ from the average GT value of the data so that it was still within acceptable limits in terms of the functionality of the proposed method. Tab.A.1, Tab.A.2 and Tab.A.3 show the values of individual images that were worked with. To better evaluate the obtained results, a Graph 7.2 was created,

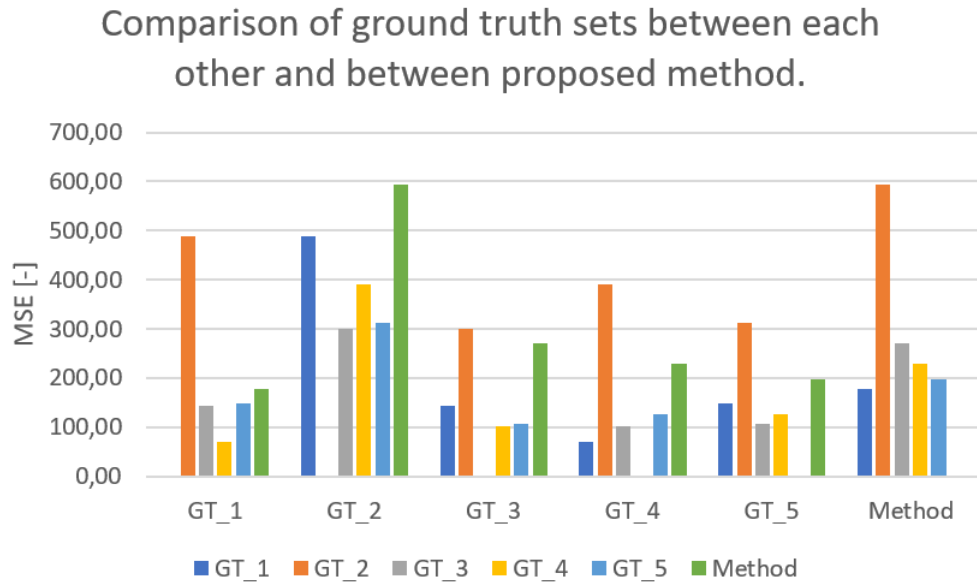


Fig. 7.1: Calculated MSE between individual ground truth datasets together with the proposed method.

which describes the difference between the determined directions of the used method and the average values of GT data. After comparing the data with GT data and taking into account the SD, the accuracy of this method is 83%.

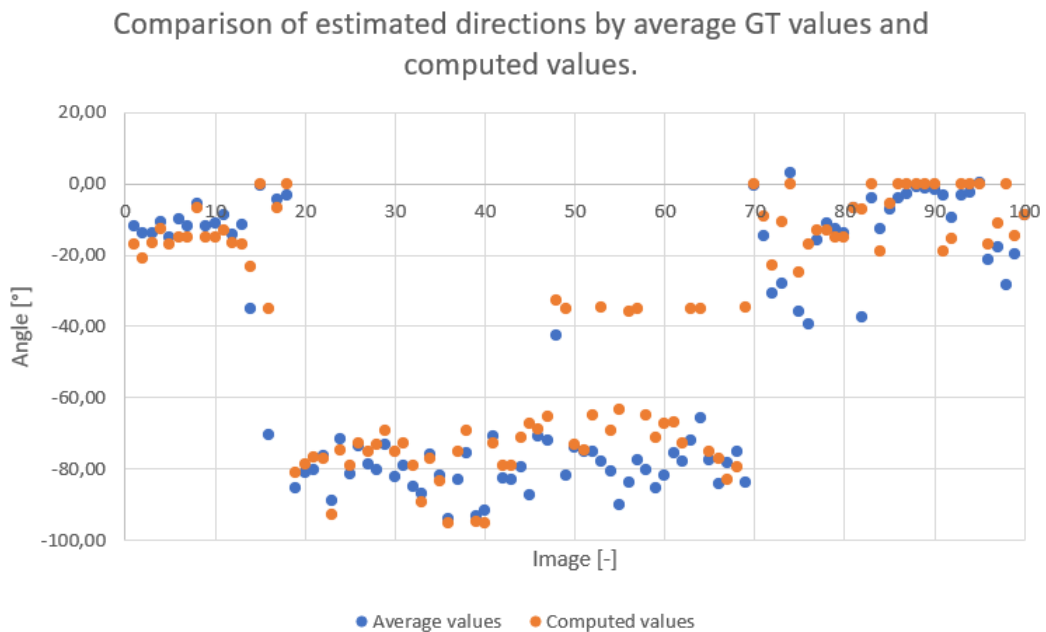


Fig. 7.2: Comparison of estimated directions by average GT values (blue dots) and computed values (orange dots).

As can be seen in Graph 7.2, the values form something like clusters, and thus the proposed method was also used to classify neurons according to their direction of growth. From the data used in this work, it was possible to determine 3 classes of directional growth, namely the class where no direction prevailed, so it was not possible to determine in which direction the neurons in the images grow. Another class were neurons that grew downwards, and the last class describes neurons that grew diagonally/square. Examples of data that belong to these classes are shown in Fig.7.3.

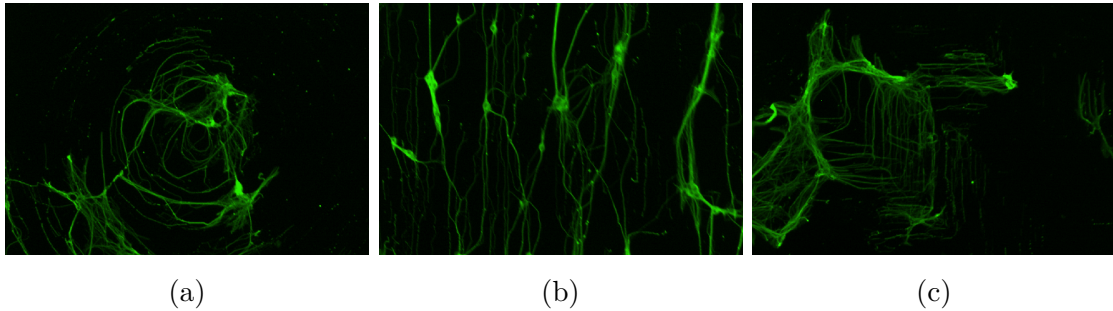


Fig. 7.3: Example of original data belonging to respective classes sorted according to the growth of the direction. a) image belonging to class 1 - no direction, b) image belonging to class 2 - vertical direction and c) image belonging to class 3 - diagonal or square direction.

The classification criterion for each image was their direction calculated by the proposed method. The Fig.7.4 shows the classification of individual images into classes, where the values of the directions of the images form clusters with similar values. A good example are images with neurons growing downwards. Since they have a growth direction around -90° , it can be seen in the figure that the data are from -60° and thus cluster at the bottom half of the Fig7.4. This classification has an accuracy of 91% and that is the reason why two classes can be seen in the Fig.7.4 around -35° . These data were misclassified due to incorrect calculation of the direction of neurite growth in the figure.

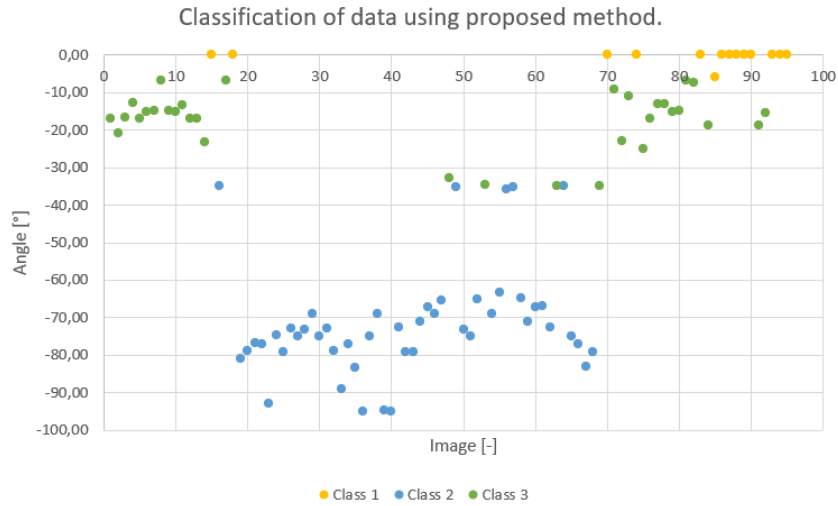


Fig. 7.4: Classification of data into individual classes according to the proposed method, where class 1 (yellow) describes data without a predominant growth direction, class 2 (blue) describes data with a downward growth direction and class 3 (green) describes data with growth diagonally or square.

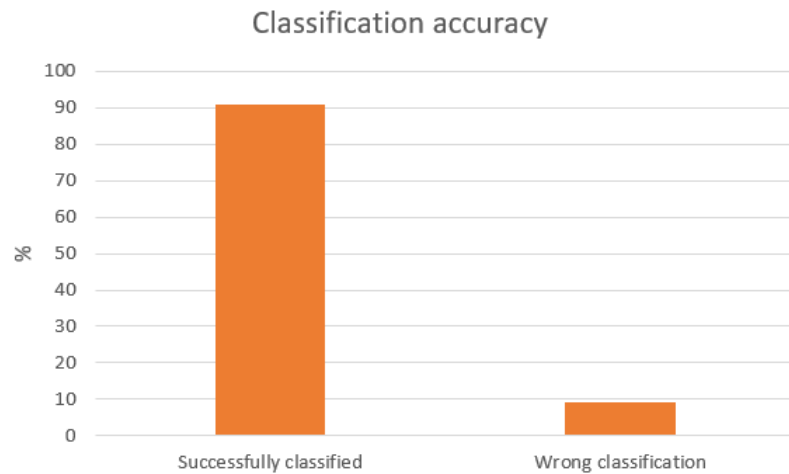
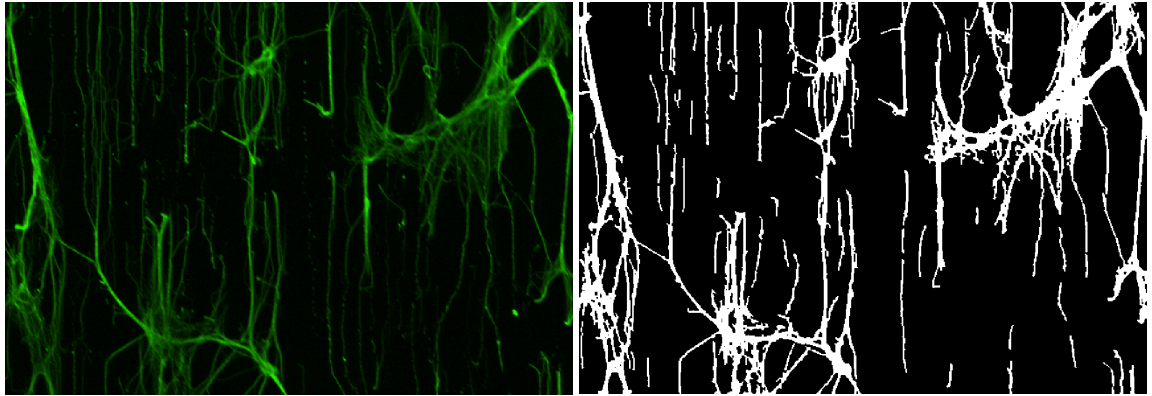


Fig. 7.5: Classification accuracy of proposed method.

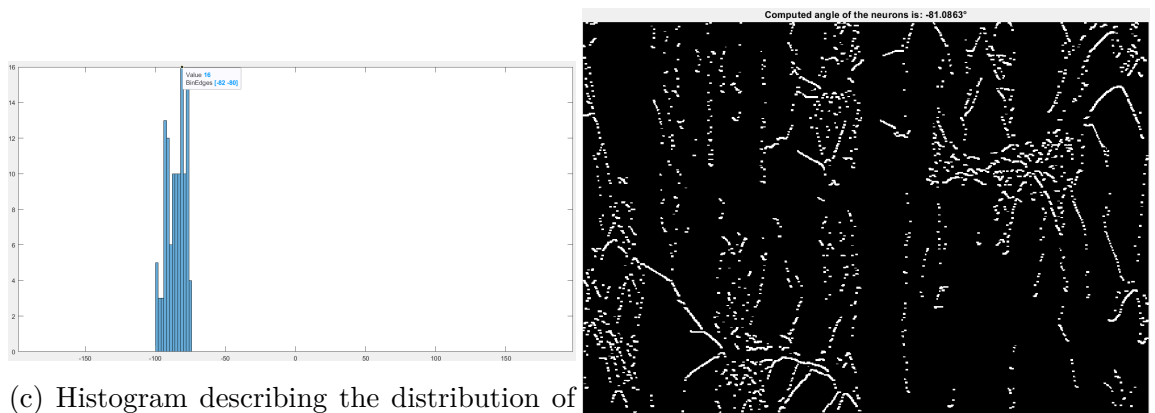
The following figures (Fig.7.6, Fig.7.7) show the correctly determined direction of neuron growth by the proposed method. The separate gradient directions were calculated from the segmented image (Fig.7.6b, Fig.7.7b). The individual values of the direction are shown on the histogram (Fig.7.6c, Fig.7.7c), where the interval with the largest number is highlighted. An average value was calculated from this interval and it describes the dominant directionality. The last images (Fig.7.6d, Fig.7.7d) show the overall direction of the gradient for the whole image, but this type of image was not worked on, it only serves as an illustration when imagining

the direction of the gradients.



(a) Input image.

(b) Segmented image.

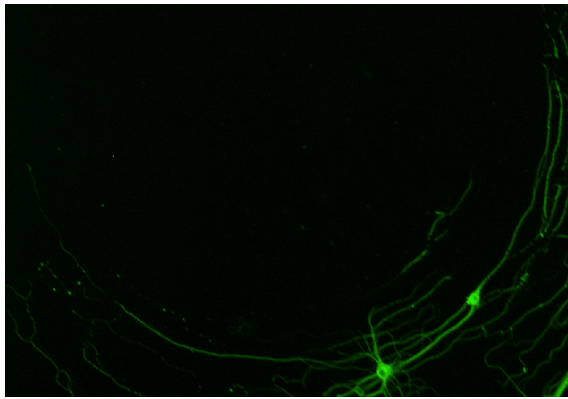


(c) Histogram describing the distribution of directions in the image.

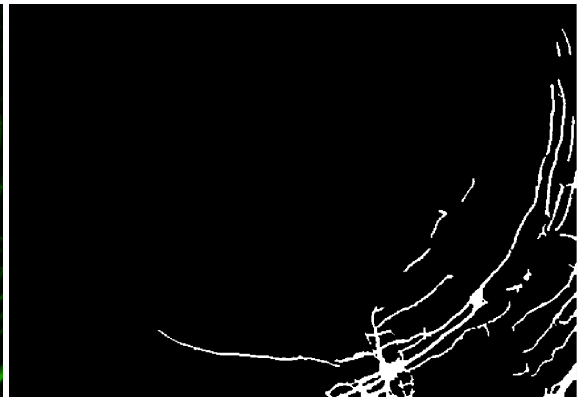
(d) Image showing gradient direction with calculated angle.

Fig. 7.6: Output after direction analysis with correctly determined direction - downward.

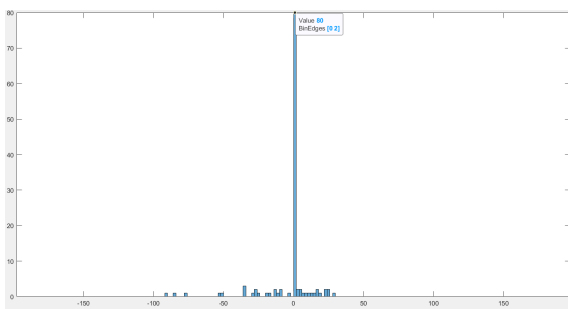
An example of data for which direction analysis failed are images (Fig.7.8a, Fig.7.9a). The procedure was the same for the whole dataset, so the gradient directions were calculated from the segmented image divided into sub-images. The reason for the error in calculating the direction in the Fig.7.8a is most likely a large cluster of dendrites in the soma region. These clusters could have increased the number in the wrong directional variable, and since this method selects the dominant direction from the most numerous variable, thus the wrong primary direction was assigned to this image. As we can see from the histogram in the Fig.7.8c, the picture contains parts that would in reality correspond to the direction of growth, but were suppressed by a larger group. The reason for the wrong determination of the direction in the Fig.7.9 is the opposite as in the previous one. GT data show no direction, but the method found some. The direction it captured probably comes again from



(a) Input image.



(b) Segmented image.



(c) Histogram describing the distribution of directions in the image.

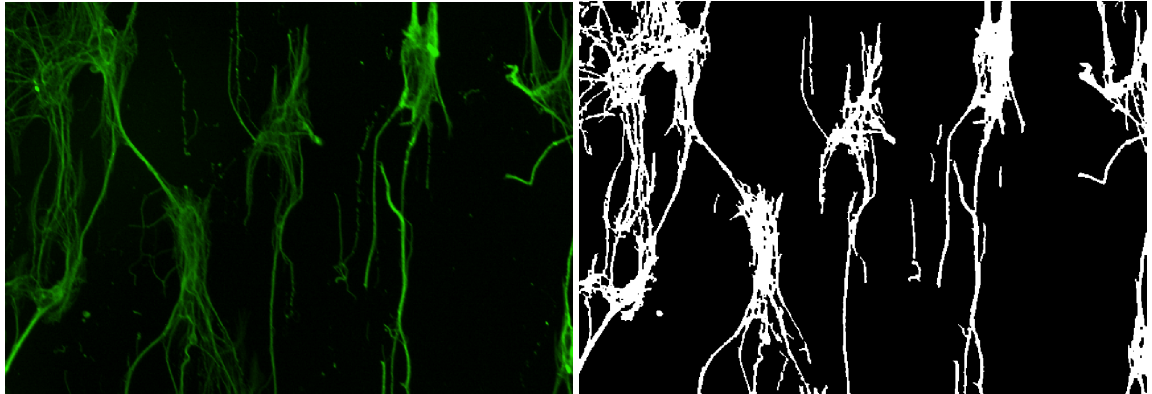


(d) Image showing gradient direction with calculated angle.

Fig. 7.7: Output after direction analysis with correctly determined direction - none.

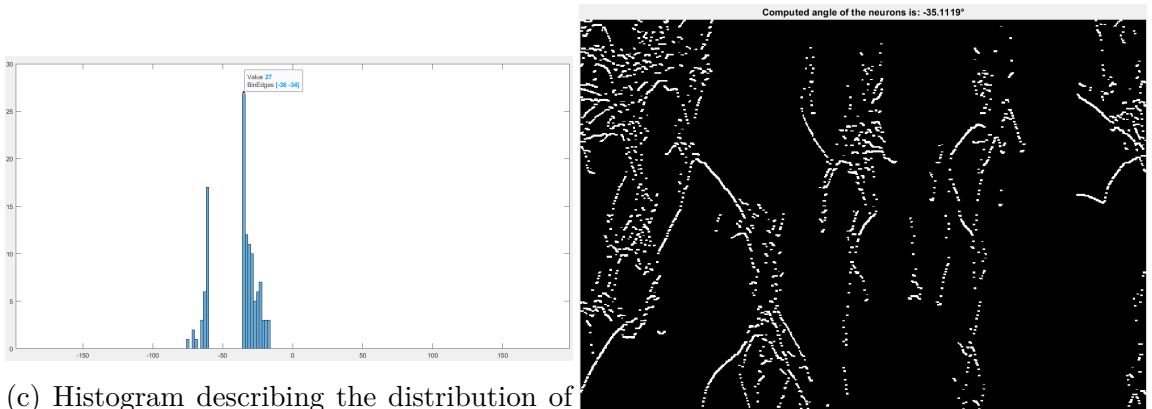
the soma (Fig.7.9b). However, since this image is marked without directionality in the GT data, the proposed analysis is incorrect.

This method is mainly dependent on the data it works with. Another example of data this method cannot be applied to is shown in the Fig.7.10. The reason for the wrong direction is in this case a large representation of different directions as seen in histogram in the Fig.7.10c. In this type of data, both the method and the individuals determining the ground truth data failed to choose prevailing direction. The standard deviation of this image between GT data takes up to 38.81. The average value of all standard deviations between all 100 images is only 8. Compared to the other data, this type is unsuitable for the proposed method simply because it is not clear in which direction the neurite is growing.



(a) Input image.

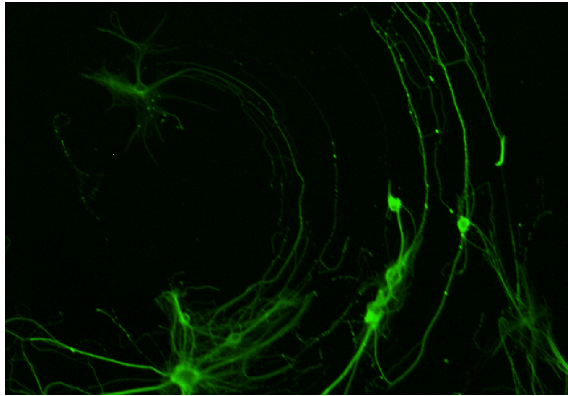
(b) Segmented image.



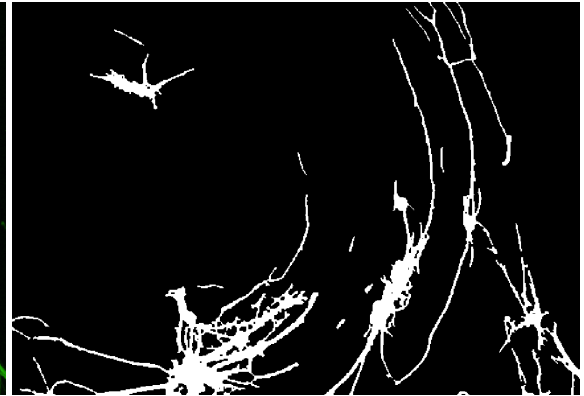
(c) Histogram describing the distribution of directions in the image.

(d) Image showing gradient direction with calculated angle.

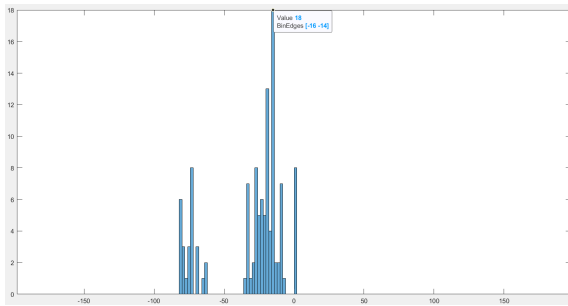
Fig. 7.8: Output after direction analysis with incorrectly determined direction.



(a) Input image.



(b) Segmented image.

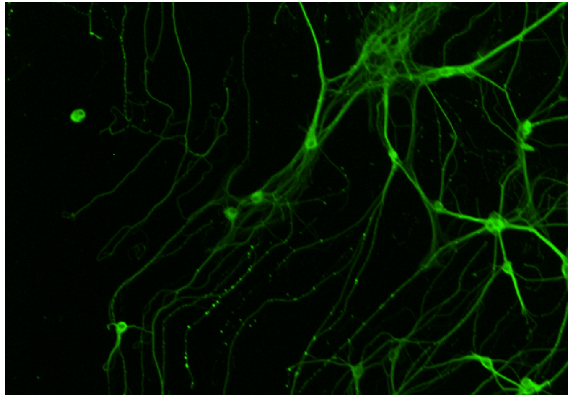


(c) Histogram describing the distribution of directions in the image.

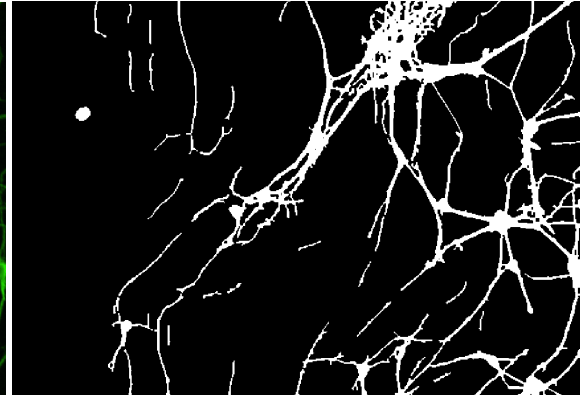


(d) Image showing gradient direction with calculated angle.

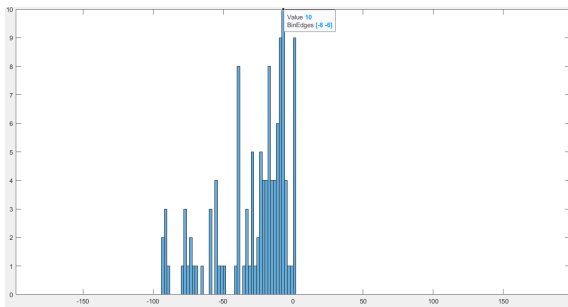
Fig. 7.9: Output after direction analysis with incorrectly determined direction.



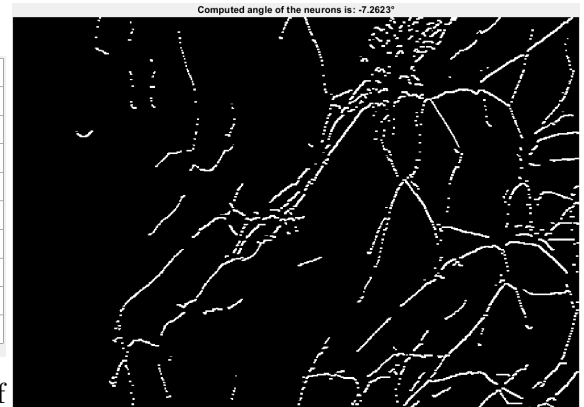
(a) Input image.



(b) Segmented image.



(c) Histogram describing the distribution of directions in the image.



(d) Image showing gradient direction with calculated angle.

Fig. 7.10: Output after direction analysis with incorrectly determined direction.

Conclusion

This master's thesis was focused on the analysis of neurite directionality using a suitable method that needed to be designed.

The first chapter describes the structure of the neuron, by which the nervous system is formed. There are described individual parts and their function.

The second chapter depicts fluorescence microscopy and its use in the observation of neurons. The principle of this technique and also the individual types, namely wide-field and confocal microscopy are explained. Labeling is necessary for proper observation of neurons, as the neuron is not autofluorescent. Basic labeling methods are also specified in this chapter.

The third chapter details the basic methods of neuronal segmentation, namely segmentation of soma and dendrites. In the case of soma segmentation, for example, Laplacian of Gauss is used, in the case of dendrites, for example, a growing region.

The fourth chapter describes neurite tracing, which may be an alternative version of segmentation.

The content of the fifth chapter is a description of the experimental data that were used in the master's thesis. There is a description of how neurons were grown and on what structures.

The sixth chapter, specifies the practical part of the master's thesis. Three different segmentation methods and one directionality analysis method were proposed.

The last, seventh chapter, describes the obtained results and their subsequent discussion. The method alone in determining growth directions compared to ground truth data had a success rate of 83%. Since there were more GT datasets, the standard deviation was estimated, which was used as a guide to determine the success limit of the calculated method directions. The applicability of this method is also in the classification. The data were divided into three groups, with a classification accuracy of 91%. At the end of the thesis, examples of data are inserted, when the proposed method was able to determine the correct direction and contrariwise, while it is described for each image, where the error in analysis could have occurred.

A possible improvement of this method and thus also the subject in the case of follow-up work would be to limit the influence of soma on directional analysis. In this case, it would be convenient to eliminate from segmentation an area of a large cluster of somas or dendrites which do not carry information about the direction of growth. Another possibility is the segmentation of a part of the neuron containing only the primary neurite, which would determine the direction of growth of the whole neuron.

Bibliography

- [1] ČECH, Svatopluk and Drahomír HORKÝ. *Histologie a mikroskopická anatomie pro bakaláře*. 2nd edition, Brno: Masarykova univerzita, 2011. ISBN 978-80-210-5544-5.
- [2] DOSTÁL, Jiří, Hana PAULOVÁ, Jiří SLANINA and Eva TÁBORSKÁ. *Biochemie pro posluchače bakalářských oborů*. Brno: Masarykova univerzita, 2012. ISBN 978-80-210-5020-4.
- [3] HRAZDIRA, Ivo and Vojtěch MORNSTEIN. *Lékařská biofyzika a přístrojová technika*. Brno: Neptun, 2001. ISBN 80-902896-1-4.
- [4] SPRING, Kenneth R. and Michael W. DAVIDSON. *Introduction to Fluorescence Microscopy*. MicroscopyU: The source for microscopy education [online]. Melville, New York: Nikon Instruments, 2020 [cit. 2020-11-17]. Available at: <https://www.microscopyu.com/techniques/fluorescence/introduction-to-fluorescence-microscopy>
- [5] DUNST, Sebastian and Pavel TOMANCAK. *Imaging Flies by Fluorescence Microscopy: Principles, Technologies, and Applications*. GENETICS. 2019, 211(1), 15-34.
- [6] PISTON, David W., George H. PATTERSON, Jennifer LIPPINCOTT-SCHWARTZ, Nathan S. CLAXTON and Michael W. DAVIDSON. *Imaging Fluorescent Proteins: Imaging Parameters for Fluorescent Proteins*. MicroscopyU: The source for microscopy education [online]. Melville, New York: Nikon Instruments, 2020 [cit. 2020-11-17]. Available at: <https://www.microscopyu.com/techniques/fluorescence/fluorescent-protein-imaging-parameters>
- [7] FENG, Guoping, Rebecca H. MELLOR, Michael BERNSTEIN, et al. *Imaging Neuronal Subsets in Transgenic Mice Expressing Multiple Spectral Variants of GFP*. Neuron [online]. 2000, 28(1), 41-51 [cit. 2020-11-18]. ISSN 08966273. Available at: doi:10.1016/S0896-6273(00)00084-2
- [8] SAKAGUCHI, Richi, Marcus N LEIWE and Takeshi IMAI. *Bright multicolor labeling of neuronal circuits with fluorescent proteins and chemical tags*. ELife [online]. 2018, 7 [cit. 2020-11-18]. ISSN 2050-084X. Available at: doi:10.7554/eLife.40350
- [9] SANDERSON, M. J., I. SMITH, I. PARKER and M. D. BOOTMAN. *Fluorescence Microscopy*. Cold Spring Harbor Protocols [online]. 2014, 2014(10),

- pdb.top071795-pdb.top071795 [cit. 2020-12-03]. ISSN 1559-6095. Available at: doi:10.1101/pdb.top071795
- [10] JAN, Jiří. *Medical image processing, reconstruction and restoration: concepts and methods*. Boca Raton: Taylor & Francis, 2006. ISBN 978-0-8247-5849-3.
- [11] PANI, Giuseppe, Winnok H. DE VOS, Nada SAMARI, Louis DE SAINT-GEORGES, Sarah BAATOUT, Patrick VAN OOSTVELDT and Mohammed Abderrafi BENOTMANE. *MorphoNeuroNet: An automated method for dense neurite network analysis*. Cytometry Part A [online]. 2014, 85(2), 188-199 [cit. 2020-12-02]. ISSN 15524922. Available at: doi:10.1002/cyto.a.22408
- [12] BAGLIETTO, Silvia, Ibolya E. KEPIRO, Gerrit HILGEN, Evelyne SER-NAGOR, Vittorio MURINO and Diego SONA. *Automatic Segmentation of Neurons from Fluorescent Microscopy Imaging*. Cham: Springer International Publishing, 2018, 2018-07-03, s. 121-133 [cit. 2020-11-30]. Communications in Computer and Information Science. ISBN 978-3-319-94805-8. Available at: doi:10.1007/978-3-319-94806-5_7
- [13] HEMALATHA, R.J., T.R. THAMIZHVANI, A. Josephin Arockia DHIVYA, Josline Elsa JOSEPH, Bincy BABU and R. CHANDRASEKARAN. *Active Contour Based Segmentation Techniques for Medical Image Analysis*. KOPROWSKI, Robert, ed. Medical and Biological Image Analysis [online]. In-Tech, 2018, 2018-07-04 [cit. 2020-12-01]. ISBN 978-1-78923-330-8. Available at: doi:10.5772/intechopen.74576
- [14] YU, Weimiao, Hwee Kuan LEE, Srivats HARIHARAN, Wenyu BU and Sohail AHMED. *Quantitative neurite outgrowth measurement based on image segmentation with topological dependence*. Cytometry Part A [online]. 2009, 75A(4), 289-297 [cit. 2020-12-01]. ISSN 15524922. Available at: doi:10.1002/cyto.a.20664
- [15] MEIJERING, E., M. JACOB, J.-C. F. SARRIA, P. STEINER, H. HIRLING and M. UNSER. *NEURITE TRACING IN FLUORESCENCE MICROSCOPY IMAGES USING RIDGE FILTERING AND GRAPH SEARCHING: PRINCIPLES AND VALIDATION*. Arlington, VA; United States: 2004 2nd IEEE International Symposium on Biomedical Imaging: Macro to Nano, 2004. ISBN 0780383885.
- [16] SLAVÍK, Jan, Vratislav ČMIEL, Jaromír HUBÁLEK, Yi YANG and Tian-Ling REN. *Hippocampal neurons alignment on quartz grooves and parylene cues on quartz substrate*.

- [17] SANKUR, Bülent and Mehmet SEZGIN. *Survey over image thresholding techniques and quantitative performance evaluation*. Journal of Electronic Imaging [online]. 2004, 13(1) [cit. 2020-12-31]. ISSN 1017-9909. Available at: doi:10.1117/1.1631315
- [18] ILLOWSKY, Barbara and Susan DEAN. *Introductory Statistics: Volume 1 of 2*. Rice University, Houston, Texas: OpenStax College, 2013. ISBN 978-1-304-89164-8.
- [19] GOWERS, Timothy, June BARROW-GREEN and Imre LEADER, ed. *The Princeton companion to mathematics*. Princeton: Princeton University Press, c2008. ISBN 978-0-691-11880-2.

List of symbols, quantities and abbreviations

EGFP Enhanced green fluorescent protein

GFP Green fluorescent protein

GT Ground truth

IF Immunofluorescence

LEDs Light-emitting diodes

LoG Laplacian of Gaussian

MSE Mean Squared Error

PMT Photomultiplier

ROIs Regions of interest

SD Standard deviation

UV Ultraviolet

List of appendices

- A Tables containing ground truth data, standard deviation and calculated values. 45

A Tables containing ground truth data, standard deviation and calculated values.

Tab. A.1: Table of average value of ground truth data, standard deviation and calculated value for images 1 -36.

Number of image									
x	1	2	3	4	5	6	7	8	9
GT	-11,77	-14,02	-14,06	-10,62	-15,08	-10,12	-11,79	-5,85	-11,79
SD	5,66	8,28	9,10	5,96	7,63	6,96	2,93	3,66	6,62
Dir.	-16,86	-20,89	-16,77	-12,66	-16,91	-15,05	-14,96	-6,84	-14,95
Number of image									
x	10	11	12	13	14	15	16	17	18
GT	-11,32	-8,67	-14,17	-11,56	-35,29	-0,66	-70,57	-4,62	-3,22
SD	5,60	4,92	3,43	9,63	25,69	0,65	11,36	1,81	3,06
Dir.	-15,20	-13,27	-16,82	-17,04	-23,38	0,00	-35,03	-6,89	0,00
Number of image									
x	19	20	21	22	23	24	25	26	27
GT	-85,22	-80,91	-80,23	-76,11	-88,92	-71,54	-81,47	-73,58	-78,77
SD	5,33	6,68	6,25	7,31	2,92	5,30	5,21	6,02	8,78
Dir.	-81,09	-78,78	-76,72	-77,09	-92,96	-74,75	-79,10	-72,92	-74,98
Number of image									
x	28	29	30	31	32	33	34	35	36
GT	-80,26	-73,24	-82,13	-79,06	-85,07	-86,94	-75,88	-81,76	-93,75
SD	8,87	8,21	7,86	6,28	9,37	2,52	1,26	6,60	3,00
Dir.	-73,25	-69,09	-75,08	-72,88	-78,91	-89,07	-77,17	-83,41	-95,03

Tab. A.2: Table of average value of ground truth data, standard deviation and calculated value for images 37 -72.

Number of image									
x	37	38	39	40	41	42	43	44	45
GT	-83,13	-75,46	-93,20	-91,70	-70,88	-82,56	-82,80	-79,45	-87,18
SD	8,56	6,31	1,83	4,44	2,64	5,31	9,60	8,11	12,09
Dir.	-75,04	-69,07	-94,79	-95,00	-72,72	-79,22	-79,08	-71,07	-67,17
Number of image									
x	46	47	48	49	50	51	52	53	54
GT	-70,66	-72,14	-42,45	-81,95	-73,82	-75,18	-75,25	-78,03	-80,43
SD	4,67	5,63	8,78	5,24	4,44	6,72	8,73	10,24	8,23
Dir.	-68,91	-65,26	-32,90	-35,11	-73,27	-74,85	-65,06	-34,69	-69,11
Number of image									
x	55	56	57	58	59	60	61	62	63
GT	-89,91	-83,56	-77,54	-80,05	-85,49	-81,71	-75,64	-77,95	-72,09
SD	6,75	11,90	16,18	8,59	4,10	11,94	10,30	11,07	10,99
Dir.	-63,19	-35,72	-35,21	-64,76	-71,00	-67,09	-66,93	-72,68	-34,91
Number of image									
x	64	65	66	67	68	69	70	71	72
GT	-65,74	-77,43	-84,26	-78,39	-75,20	-83,86	-0,75	-14,85	-30,91
SD	8,43	9,60	5,28	4,62	6,75	8,74	1,21	6,84	17,56
Dir.	-35,03	-75,06	-77,09	-82,97	-79,29	-34,87	0,00	-9,18	-23,04

Tab. A.3: Table of average value of ground truth data, standard deviation and calculated value for images 73 -100.

Number of image									
x	73	74	75	76	77	78	79	80	81
GT	-28,15	2,77	-35,74	-39,25	-16,04	-11,25	-12,70	-13,86	-7,00
SD	19,54	5,36	13,69	23,29	6,99	5,32	8,69	7,30	5,74
Dir.	-10,95	0,00	-25,06	-17,02	-12,98	-13,06	-15,20	-15,00	-6,89
Number of image									
x	82	83	84	85	86	87	88	89	90
GT	-37,43	-3,96	-12,93	-7,30	-3,91	-3,00	-0,82	-1,33	-1,85
SD	38,81	4,10	6,50	6,51	2,87	2,51	0,71	1,52	1,61
Dir.	-7,26	0,00	-18,87	-5,77	0,00	0,00	0,00	0,00	0,00
Number of image									
x	91	92	93	94	95	96	97	98	99
GT	-3,14	-9,59	-3,36	-2,41	0,04	-21,39	-17,76	-28,61	-19,70
SD	2,35	7,81	2,74	2,54	1,30	16,01	10,65	19,69	10,85
Dir.	-18,87	-15,39	0,00	0,00	0,00	-17,00	-11,01	0,00	-14,79
Number of image									
x	100								
GT	-8,81								
SD	6,28								
Dir.	-8,92								